Ahmed El-Rafei, Tobias Engelhorn, Simone Wärntges, Arnd Dörfler, Joachim Hornegger, Georg Michelson. A framework for voxel-based morphometric analysis of the optic radiation using diffusion tensor imaging in glaucoma. Magnetic resonance imaging 1 October 2011 (volume 29 issue 8 Pages 1076-1087 DOI: 10.1016/j.mri.2011.02.034)

A Framework for Voxel-Based Morphometric Analysis of the Optic Radiation Using Diffusion Tensor Imaging in Glaucoma

Ahmed El-Rafei[a,b,*], Tobias Engelhorn[c], Simone Wärntges[d,e], Arnd Dörfler[c], Joachim Hornegger[a,b], Georg Michelson[b,d,e]

[a] *Pattern Recognition Lab, Department of Computer Science*
[b] *Erlangen Graduate School in Advanced Optical Technologies (SAOT)*
[c] *Department of Neuroradiology*
[d] *Department of Ophthalmology*
[e] *Interdisciplinary Center of Ophthalmic Preventive Medicine and Imaging, Friedrich-Alexander-University Erlangen-Nuremberg, Erlangen, Germany*

Keywords: Diffusion Tensor Imaging, Glaucoma, Optic Radiation, Voxel-Based Morphometry

[☆] Abbreviations: DTI, Diffusion Tensor Imaging.

[*] Corresponding author. Address: Pattern Recognition Lab, Department of Computer Science, Friedrich-Alexander-University Erlangen-Nuremberg, Martensstr. 3, 91058 Erlangen, Germany. Tel.: +49 9131 85 27775; fax: +49 9131 303811.

Email addresses: ahmed.el-rafei@informatik.uni-erlangen.de (Ahmed El-Rafei), tobias.engelhorn@uk-erlangen.de (Tobias Engelhorn), simone.waerntges@uk-erlangen.de (Simone Wärntges), arnd.doerfler@uk-erlangen.de (Arnd Dörfler), joachim.hornegger@informatik.uni-erlangen.de (Joachim Hornegger), georg.michelson@uk-erlangen.de (Georg Michelson)

URL: http://www5.informatik.uni-erlangen.de/en/our-team/el-rafei-ahmed (Ahmed El-Rafei)

Abstract

Glaucoma is an optic neuropathy affecting the entire visual system. The understanding of the glaucoma mechanism and causes remains unresolved. Diffusion tensor imaging (DTI) has been used to analyze the optic nerve and optic radiation showing global fiber abnormalities associated with glaucoma. Nevertheless, the complex structure of the optic radiation and the limitations of DTI make the localization of the glaucoma effect a difficult task. The aim of this work is to establish a framework for the determination of the local changes of the optic radiation due to glaucoma using DTI. The proposed system utilizes a semi-automated algorithm to produce an efficient identification of the optic radiation. Segmented optic radiations are transformed to a unified space using shape-based non-rigid registration. Using the deformation fields that resulted from the registration, the maps of the diffusion tensor-derived parameters are transformed to the unified space. This allows for statistical voxel-wise analysis to produce significant abnormality maps. The proposed system is applied to a group of 13 glaucoma patients and a normal control group of 10 subjects. The groups are age matched to eliminate the age effect on the analysis. Diffusion related parameters (axial, radial, and mean diffusivities) and an anisotropy index (fractional anisotropy) are studied. The anisotropy analysis indicates that the majority of the significant voxels show decreased fractional anisotropy in the glaucoma patients compared to the control group. Additionally, the significant regions are mainly distributed in the middle (in reference to anterior-posterior orientation) of the optic radiation. Glaucoma subjects have increased radial diffusivity and mean diffusivity significant voxels with a main concentration in the proximal part of the right optic radiation. The proposed analysis provides a framework to capture the significant local changes of the optic radiation due to glaucoma. The preliminary analysis suggests that the glaucomatous optic radiation may suffer from localized white matter degeneration. The framework facilitates further studies and understanding of the pathophysiology of glaucoma.

1. Introduction

Glaucoma is an optic neuropathy accompanied by visual disorder. It is usually associated with damage of the retinal ganglion cells and the optic nerve fibers which are responsible for transmitting the visual information from the eye to the brain [1]. The progression of glaucoma results in visual impairment that can reach complete vision loss if untreated. It is the second leading cause of blindness in the world affecting more than 60 million people and 8.4 million people suffering from bilateral blindness [2]. The vision loss due to glaucoma is irreversible but if glaucoma is detected in an early stage, the progression of glaucoma can be delayed or stopped.

As a systemic disease, glaucoma generally affects the entire visual system. The human visual system consists of two major components, the eye and the visual pathway inside the brain. The visual information captured by the photoreceptors is transmitted through the retinal ganglion cells and their axons, comprising the retinal nerve fiber layer, to the brain. The visual pathway continues in the brain through the optic nerve projecting from the retina through the optic chiasm and optic tracts to the lateral geniculate nucleus (LGN). The optic radiation is a densely packed bundle of myelinated axons that projects from the LGN to the primary visual cortex. The primary visual cortex is responsible for the processing of the visual information [3, 4].

In experimental glaucoma the degeneration has been shown to be transsynaptic. i.e., atrophy is transmitted from diseased neurons to healthy nerve cells through synaptic connections [5]. The neuronal degeneration of glaucoma was shown to extend to different parts of the visual pathway spreading to the intercranial optic nerve, lateral geniculate nucleus and visual cortex [6]. The integrity of the white matter fibers of the optic nerve and the optic radiation is reported to be globally decreased assessed by diffusion related parameters based on diffusion tensor imaging [7, 8]. Therefore, neuroimaging techniques such as diffusion tensor imaging (DTI), allowing for non-invasive in-vivo white matter fiber identification and quantification, have a great potential in the understanding of neuronal diseases such as glaucoma.

Despite the extensive research on glaucoma and the valuable findings, the causes of glaucoma remain uncertain and the pathophysiology mechanism is not yet fully understood. Localizing the glaucoma effect on the visual system could provide more insight into the mechanism and progression of glaucoma. To the authors' knowledge, the effect of glaucoma on the optic radiation is studied through diffusion tensor-derived parameters only globally and it has

not been localized so far. The complexity of diffusion tensor imaging accompanied by inherited uncertainty and the complicated inter-subject variable structure of the optic radiation make localizing the effect of glaucoma on the optic radiation a difficult task. In this work, we propose a framework that is able to capture the local changes of the optic radiation due to neuronal diseases. The framework is applied to the glaucoma disease. The optic radiation is identified on diffusion tensor images. The diffusion process is sensitive to the underlying fiber structure, and consequently the diffusion tensor-derived parameters are expected to change in cases of white matter tracts damage due to neurological disorders. Thus, they are commonly utilized to detect the degradation in the cerebral white matter health when examining pathologies [9, 10, 11, 12].

The proposed framework for the localization of the glaucomatous damage on the optic radiation is object oriented. It processes the optic radiation rather than the whole brain. Whole brain analysis is subject to many sources of inaccuracies and therefore avoided. The framework uses a semi-automated algorithm for identifying the optic radiation to limit the user intervention and increase the reliability of the results. In addition, relying on diffusion tensors or related parameters in the calculation of the similarity in the registration step is not suitable for dealing with glaucoma. This is because different parameters were shown to be affected by glaucoma and consequently the whole diffusion tensors. Thus, an automated shape-based registration approach is incorporated to overcome this limitation. The analysis is restricted to the main fiber bundle of the optic radiation where there is a high degree of shape similarity. This simplifies and facilitates the registration leading to improved inter-subject alignments.

2. Background and Related Work

The Brownian motion of the water molecules within white matter fibers is restricted by the cell membranes and myelin sheaths surrounding the axons. Diffusion weighted imaging (DWI) relies on modulating the magnetic resonance signal by the self-diffusion of the water like molecules. The most common mathematical formalism for extracting quantitative data from the diffusion process is the diffusion tensor [13, 14, 15]. The diffusion within a voxel is modeled as a Gaussian process and represented by a diffusion tensor.

The spectral decomposition of the diffusion tensor leads to information regarding the local fiber orientation, which is assumed to coincide with the

principal diffusion direction (PDD) in simple regular fiber structure. Moreover, parameters have been derived from the diffusion tensor to describe different aspects of the diffusion process. Diffusivity is described along the PDD by the axial diffusivity (AD) and perpendicular to the PDD by the radial diffusivity (RD). The average diffusivity within a voxel is characterized by the mean diffusivity (MD). Increased radial diffusivity is hypothesized to reflect the demyelination degree and this assumption was validated in clinical studies on mouse brain [11, 16] while MD represents the magnitude of the diffusion within a voxel. Fractional anisotropy (FA) [17] indicates the degree of deviation from isotropic diffusion at each voxel. In clinical applications, FA is widely assumed to represent the organization degree of white matter fibers reflecting white matter integrity. Reduced FA values could be interpreted as compromised fiber coherence (degree of cellular structure alignment within a voxel) and possible defects in myelin [9, 10, 12].

Diffusion tensor imaging opened a new dimension in the field of neuroimaging enabling the reconstruction of the brain white matter structure in-vivo [18, 19]. It allows for building an atlas of white matter fibers [20]. Moreover, DTI received a lot of attention due to its clinical applications. Among DTI applications [21] are the ability of diffusion weighted imaging to early detect cerebral diseases such as acute strokes [22, 23] as well as the demonstrated sensitivity of diffusion tensor-derived parameters to different neuropathologies including Alzheimer disease [24, 25] and multiple sclerosis [26].

Different approaches exist for tracking the white matter fibers from DTI data. Algorithms were developed to reconstruct the human visual pathway [27] and to identify parts of it such as the optic radiation [28, 29]. This enables the analysis of the effects of ophthalmological and systemic neurological diseases on the visual pathway.

Analysis of diseases using DTI follows two major approaches. The analysis is performed between a diseased group and a control group. Histogram analysis represents the first approach and is based on statistically analyzing the different features of the histogram of diffusion tensor-derived parameters on a specified region of interest [30, 31]. Features of the histogram may include mean, median, location of the peak, etc. This approach gives the global significant differences between the two examined groups but it lacks the ability to localize these differences. Voxel-based morphometric analysis examines the local changes of tensor derived-parameters to produce a map of significant abnormalities in the presence of neurological diseases such as

optic neuritis, amyotrophic lateral sclerosis [32, 33]. Studying hemispheric asymmetry due to aging effect or pathologies such as schizophrenia is another application of voxel-based analysis [34, 35, 36].

Voxel-based morphometry (VBM) is commonly used in a whole brain analysis for localizing the abnormalities in the presence of pathologies. Brain images from different subjects involved in the study are transformed to a unified coordinate system by registering them to a template. This allows for inter-subject voxel-wise comparisons because each location in the unified coordinate system should include corresponding voxels from all subjects. Due to the complex structure of the brain and the highly inter-subject brain structure variability, the registration is imperfect and significant voxels could arise from the misalignment of images. Smoothing is incorporated to reduce the inter-subject variability and misalignments by replacing the image intensity value by a weighted average from neighboring voxels. Smoothing increases the partial volume effects. Previous study showed that the morphometry analysis depends on the degree of smoothing [37]. Tract-based spatial statistics (TBSS) approach is proposed to avoid the mentioned problems of conventional VBM [38]. This approach is one of the well established and applied techniques in morphometry analysis using DTI. TBSS operates on FA images in a multi-step method. First, the FA brain images from different subjects are aligned using non-rigid registration. Then, the mean of the registered FA images is computed and a skeleton of the white matter tracts is calculated from it. Finally, the different subjects are projected onto this alignment invariant tract and the statistical analysis is performed on the voxels of the skeleton. TBSS does not require smoothing and is completely automated and thus observer independent. However, TBSS processes FA images which are affected by white matter degeneration caused by diseases such as glaucoma. The spatial accuracy of the TBSS analysis is limited by the skeleton and therefore does not provide detailed significant locations. In addition, it compares skeletons of the extremely variable complete brain white matter structures.

3. Materials

3.1. Subjects

The performed case-control study included 23 subjects categorized into control and glaucoma groups. The control group consisted of 10 subjects

(3 males and 7 females with a mean age of 62.8±13.6 years) while 13 patients (6 males and 7 females with a mean age of 64.7±11.5 years) diagnosed with primary open angle glaucoma (7 patients) and normal tension glaucoma (6 patients) constituted the glaucoma group. Subjects in both groups were randomly selected from the patients in the clinic of the Department of Ophthalmology at the University Erlangen-Nuremberg. The criteria for primary open angle glaucoma (POAG) diagnosis were having an intraocular pressure (IOP) > 21 mmHg associated with an open anterior chamber angle, optic disk cupping and visual field defects > 2 dB. Criteria for diagnosis of normal tension glaucoma were the same as POAG except for an IOP < 21 mmHg. The subjects in the normal groups did not show any abnormalities of the glaucoma specific examination results. The acquired magnetic resonance imaging (MRI) and DTI datasets were utilized for neurological examinations to detect cerebral diseases or irregularly developed optic radiations.

3.2. Magnetic resonance and diffusion tensor imaging

A 3T high-field scanner (Magnetom Tim Trio, Siemens, Erlangen, Germany) was used to obtain anatomical T1-weighted images using 3D-MPRAGE imaging sequence. The strength of the applied gradient field was up to 45 mT/m (72 mT/m effective). The imaging sequence parameters were TR = 900 ms, TE = 3 ms, and field of view (FoV) = 23×23 cm^2. The acquisition matrix size = 512×256 reconstructed to 512×512 with interslice resolution of 1.2 mm.

Diffusion weighted images were acquired along 20 directions using a maximal b-factor of 1,000 s/mm^2. Additional non-diffusion weighted scan was performed with b = 0. The scanning image sequence protocol was a single-shot, spin echo, echo planar imaging (EPI) with TR = 3,400 ms, TE = 93 ms, FoV = 23×23 cm^2, and partial Fourier acquisition = 60%. The acquisition matrix size was 128×128 reconstructed to 256×256 and the number of signal averages was 4. The axial intra-slice spatial resolution was 1.8×1.8 mm^2 with a slice thickness of 5 mm.

4. Methods

The schematic of the proposed framework is illustrated in Figure 1. The main idea of the system is to spatially normalize the optic radiations from different subjects to a unified space. The identification of the optic radiation is performed automatically. The analysis is confined to the main bundles of

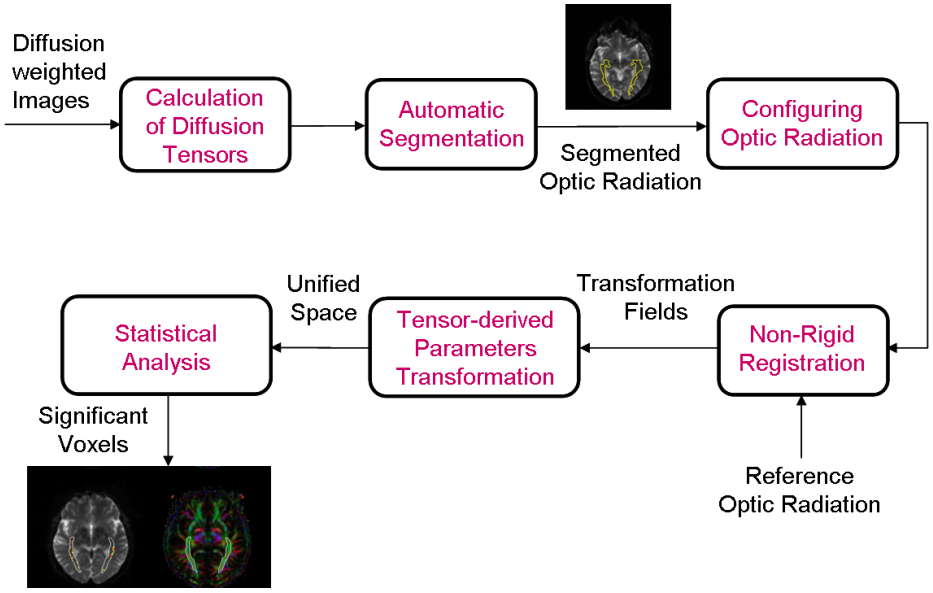

Figure 1: Schematic of the analysis framework. The system analyzes the diffusion tensor images of the optic radiation to produce localization maps showing regions with significant differences between glaucoma and control groups. The schematic illustrates the different steps including optic radiation identification and configuration, registration, and statistical analysis.

the optic radiation. Thus, the inter-subject variability is reduced to be able to accurately compare the fiber bundles from different subjects. This is done manually by removing the highly variable fiber structures and correcting the segmentation errors. The segmented optic radiations from all subjects are non-rigidly registered to a reference template. After the registration, all the segmented regions occupy the same space enabling location-based analysis. The diffusion tensor-derived parameters' images are transferred to the common space using the transformation fields obtained from the registration step. Finally, a statistical analysis is performed to detect the regions which show significant differences between glaucomatous and normal optic radiation groups. The software used in this work was mainly developed by the authors under the Matlab environment (Mathworks, Inc., Natick, MA, USA). In the following subsections, the various steps are described in detail.

4.1. Automated identification of the optic radiation

The diffusion tensors were calculated from the diffusion weighted images. The brain images were interpolated by upsampling the diffusion tensors at non-grid locations. The individual components of the diffusion tensors were trilinearly interpolated in the Log-Euclidean space [39]. The spectral components of the interpolated diffusion tensors were obtained using eigenvalue decomposition. The decomposition results included the eigenvalues of the interpolated diffusion tensors which were used to calculate the diffusivity parameters (AD, RD, and MD) and the anisotropy index (FA) using the following equations:

$$AD = \lambda_1 \tag{1}$$

$$RD = \frac{\lambda_2 + \lambda_3}{2} \tag{2}$$

$$MD = \lambda = \frac{(\lambda_1 + \lambda_2 + \lambda_3)}{3} \tag{3}$$

$$FA = \sqrt{\frac{3}{2}} \frac{\sqrt{(\lambda_1 - \lambda)^2 + (\lambda_2 - \lambda)^2 + (\lambda_3 - \lambda)^2}}{\sqrt{\lambda_1^2 + \lambda_2^2 + \lambda_3^2}} \tag{4}$$

where λ_1, λ_2 and λ_3 are the diffusion tensor eigenvalues in descending order.

The previously developed algorithm for automated segmentation of the optic radiation based on DTI data by El-Rafei et al. [29] was used to identify the optic radiation. The algorithm is automated and thus eliminates the necessity for user intervention avoiding inter-user variability. Moreover, the ability of the algorithm to identify the optic radiation in both normal and glaucoma subjects with high efficiency was demonstrated by El-Rafei et al. [29]. Therefore, it is suitable to be incorporated into the proposed framework and specifically for the glaucoma analysis.

The segmentation algorithm was applied as follows: First, the DTI images were filtered anisotropically for reducing the noise and incrementing the coherency within the fiber bundle of the optic radiation while maintaining the bundle edges. This was performed by applying a Perona-Malik filter [40] to the individual elements of the diffusion tensors. After the filtering step,

the optic radiation was initialized. Physiological properties of the optic radiation such as the dominant main diffusion direction were used to delineate the optic radiation automatically. In this step, the voxels with dominant anterior-posterior directions were identified and connectivity analysis was performed. Only voxels with high anisotropy (FA values greater than 0.3) were considered in this analysis. The optic radiation was initially identified as the largest connected object with dominant anterior-posterior diffusion direction. Then, the estimated optic radiation initialized a statistical level set engine that was iteratively evolved to produce the segmented optic radiation. The level set formulation was based on partitioning the image space into foreground (the optic radiation) and background (the remaining image space). The posterior probabilities of partitioning were modeled as Gaussian distributions within each partition. The level set was evolved by seeking the optimal segmentation that maximized the posterior probability while preserving the smoothness of the segmentation [41]. The level set formulation was extended to work with the Log-Euclidean framework. This maintained the simplicity of the calculations and speed efficiency while avoiding the drawbacks of the Euclidean framework when dealing with the diffusion tensor space. Finally, the mid brain was roughly identified and its relative position to the optic radiation was utilized to refine the segmentation eliminating anterior connected coherent tracts such as the optic tracts. A sample of a segmented optic radiation is demonstrated on an axial brain slice in Figure 2.

4.2. Configuring the optic radiation

In the axial slice that includes the largest part of the LGN and clearly identifies the intersection between the optic tracts and the optic radiation, there is a high degree of shape similarity of the optic radiation among normal and glaucoma subjects. Therefore, it was selected for further analysis. The manual configuration targeted the minimization of the inter-personal variability by restricting the analysis to the main fiber bundle of the optic radiation in order to benefit from the shape similarity between subjects. The results of the segmentation were compared to a white matter Atlas reconstructed using DTI [42]. The comparison showed that most of the errors were over-segmentation errors. The occipital part of corpus callosum medially proceeding the optic radiation and traces of the optic tracts were included in the segmentation. Based on the comparison, the segmentation errors were manually corrected by two DTI experts.

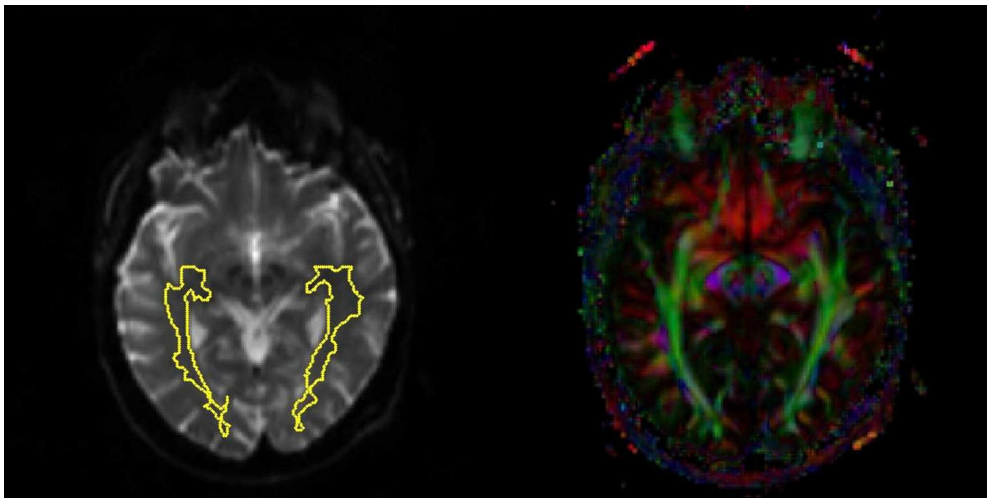

Figure 2: Sample automated segmentation of the optic radiation on an axial brain slice. The left side shows the segmented optic radiation on a non-diffusion weighted image (b=0). The corresponding diffusion direction color coded image weighted with fractional anisotropy is shown on the right side. The structure of the part of the visual pathway representing the main fiber bundle of the optic radiation and the lateral geniculate nucleus (LGN) is clearly captured.

The LGN is a small object relative to the limited spatial resolution of the DTI data. Thus, its appearance differs among different subjects which results in shape inconsistency and could lead to inaccuracies in the registration. Therefore, the lateral geniculate nuclei were excluded from the analysis and manually removed from the segmentation. The lateral geniculate nuclei can be easily identified by tracing the optic radiation and locate its intersection with the optic tracts near the anterior end of the optic radiation. The branching part of the optic radiation to the primary visual cortex was eliminated from the analysis due to significant inter-subject variability and measurement uncertainties in this region.

The complex structure of the white matter fibers complicates the configuration process. Moreover, measurement uncertainties arise from partial volume effects as well as limitation of the diffusion tensor model in describing complex fiber situations such as branching or crossing of fibers. Indices were developed to distinguish between prolate, oblate and spherical tensors [43]. Prolate tensors characterize homogeneous regions with high anisotropy and relatively high certainty of fiber orientation coincidence with the PDD. In

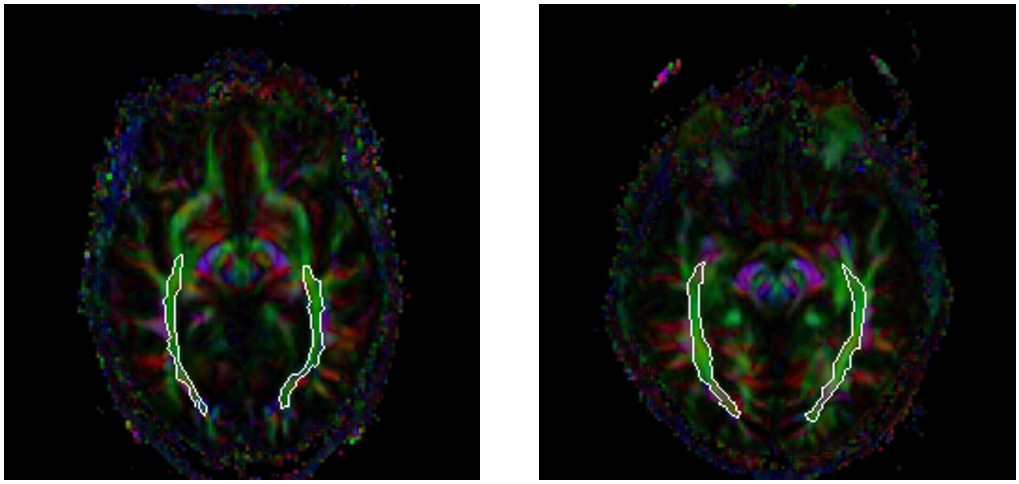

Figure 3: The optic radiation on an axial brain slice of two sample subjects after the manual segmentation. The lateral geniculate nucleus (LGN) and the branching to the visual cortex were removed.

contrast, intravoxel crossing and branching fibers result in reduced average anisotropy and uncertainty of the underlying fiber orientation. These situations are characterized by oblate tensors. To reduce the inter-operator variability and to systematize the configuration process, a graphical user interface (GUI) was developed to facilitate the user interactions. The GUI enables accurate manipulation of the segmentation results on a variety of DTI-derived measures including FA, MD, linear anisotropy (CL) and planar anisotropy (CP) images as well as principal diffusion direction color coded images. Thresholding of the mentioned parameters can be performed to visualize only the voxels above or below a certain parameter value. This can be used in conjunction with the linear and planar anisotropy indices to localize branching and intersecting fibers of the optic radiation and facilitate the manipulation procedure. For example, the branching parts of the optic radiation can be identified in a systematic way by increasing CL threshold gradually until the branching fibers are disconnected from the main fiber bundle of the optic radiation. Then these parts can be manually eliminated. Segmented optic radiation can be visualized on the anatomical diffusion weighted images for further comparison with the known anatomy.

4.3. Registration

The optic radiations from different subjects were transformed to a unified space of a reference template. This allowed for voxel-wise comparison and in turn significant region analysis. The sizes of the segmented optic radiations from different subjects were calculated and the normal subject with the maximum optic radiation area in the LGN-slice was selected as the reference subject. A non-rigid registration [44] was incorporated to transform the optic radiations from all the subjects into the reference optic radiation space. The used non-rigid registration algorithm did not require any landmarks and was fully automated. The transformation consisted of two parts representing an affine transform and a free-form deformation (FFD). The affine transform modeled the global mapping between the subject to be registered and the reference while the free-form deformation modeled the finer local mapping. In the affine transform, 12 degrees of freedom were utilized to account for the translation, rotation, scaling and shearing. Prior to the FFD calculation, the optimal affine transformation was estimated by minimizing the sum of squared differences (SSD) between the binary masks of the optic radiations from the subject to be registered and the reference subject. In the free-form deformation part, B-splines were used to describe the image domain. The B-splines were calculated on a mesh of control points covering the image domain. The deformation of the mesh points deformed the corresponding B-splines and consequently the shape of the optic radiation. The FFD transformation was obtained by optimizing the locations of the mesh control points in order to maximize a cost function that corresponded to the image similarity based on the SSD between images. The cost function also included a smoothing term to ensure the smoothness of the free-form transformation. The optimization of the cost function was performed in a hierarchical approach by decreasing the spacing between the mesh control points to align coarse to fine structures. The hierarchical optimization along with the smoothing term in the cost function provided smooth deformation fields and preserved the topology of the optic radiations. The registration operated on the binary masks of the segmented optic radiation from different subjects to align them with the binary mask of the reference optic radiation. The transformation fields for each subject were stored. Working with binary images made the registration independent from the diffusion tensors affected by glaucoma and focused on the shape similarity.

4.4. Transformation of the diffusion tensor-derived parameters to the unified space

The transformation fields obtained from registration were used to transform the diffusion tensor-derived diffusivity parameters (axial, radial and mean diffusivities) and the fractional anisotropy to the unified space. This enabled voxel-wise comparison between the normal and glaucoma groups with regard to all examined parameters.

4.5. Statistical analysis

For each of the tensor-derived parameters, each voxel in the reference optic radiation was analyzed using nonparametric Wilcoxon rank sum test. A minimal smoothing was applied to the diffusion tensor indices prior to the statistical analysis using a 3×3 Gaussian filter with a standard deviation of 0.5. The voxels were considered to show a significant difference with respect to the parameter under investigation if the p-value (uncorrected for multiple comparisons) was less than 0.05 corresponding to 95% confidence interval.

4.6. Reliability assessment of the inter-operator configuration of the optic radiation

The manual configuration of the automatically segmented optic radiation is operator dependent. Inter-operator variabilities could arise leading to false significant regions. Thus, the inter-operator reliability needs to be evaluated. The automatically segmented optic radiation was demonstrated on the GUI created by the authors to two experts in the visual system neuroanatomy and diffusion tensor imaging. The experts performed independently the manual configuration of the optic radiation to remove the branching parts of the optic radiation to the primary visual cortex and to remove the LGN. The directional color coded fractional anisotropy images were used as the basis for the manipulation process with the possibility to examine the other tensor-derived indices maps or anatomical images. The operators utilized the GUI capabilities to threshold the anisotropy indices and to monitor the branching regions of the optic radiation for a systematic approach for the manual manipulation. The final optic radiations identified by both operators were compared using the percentage of voxel overlap [45] using the following equation:

$$Overlap(\%) = \frac{V_{ox1} \cap V_{ox2}}{V_{ox1}} \times 100 \tag{5}$$

where V_{ox1} and V_{ox2} are the processed optic radiations from the first and the second operators, respectively.

The percentage of voxel overlap along with the intersection to union ratio (IUratio) [45] as given by Eq. (6) were calculated for each subject and used to evaluate the reliability between operators.

$$IUratio(\%) = \frac{V_{ox1} \cap V_{ox2}}{V_{ox1} \cup V_{ox2}} \times 100 \tag{6}$$

A third alternative metric for assessing the matching between the manipulated optic radiations from the two operators was the modified Hausdorff distance (MHD) [46]. The directed modified Hausdorff measure $d(A, B)$ between region A and region B is the average of the Euclidean distances between each point on the boundary of A to its nearest neighbor on the boundary of B. The modified Hausdorff distance is the maximum of the directed distances $d(A, B)$ and $d(B, A)$.

4.7. Evaluation of registration accuracy

An important aspect of the proposed framework is the ability of the registration algorithm to align the optic radiations from different subjects to the reference. The residuals of the registration were used to represent the degree of misalignment between the registered subjects and the reference. The overlap, the intersection to union ratio and the modified Hausdorff distance between the reference and the registered optic radiations were used as measures of the registration accuracy as well as the post-registration degree of alignment.

5. Results

DTI-brain scans of the subjects were performed. The proposed framework was applied to the DTI datasets and the significant regions were extracted. Figure 4 shows the reference optic radiation and the regions that indicated significant differences with respect to the fractional anisotropy, radial and mean diffusivities.

The FA analysis showed that the glaucoma group had mainly significant voxels with decreased fractional anisotropy in comparison to the normal group. Moreover, the significant differences were located in the middle part with regard to anterior-posterior orientation of the optic radiation as shown in Figure 5. Radial and mean diffusivities had localized higher values in the

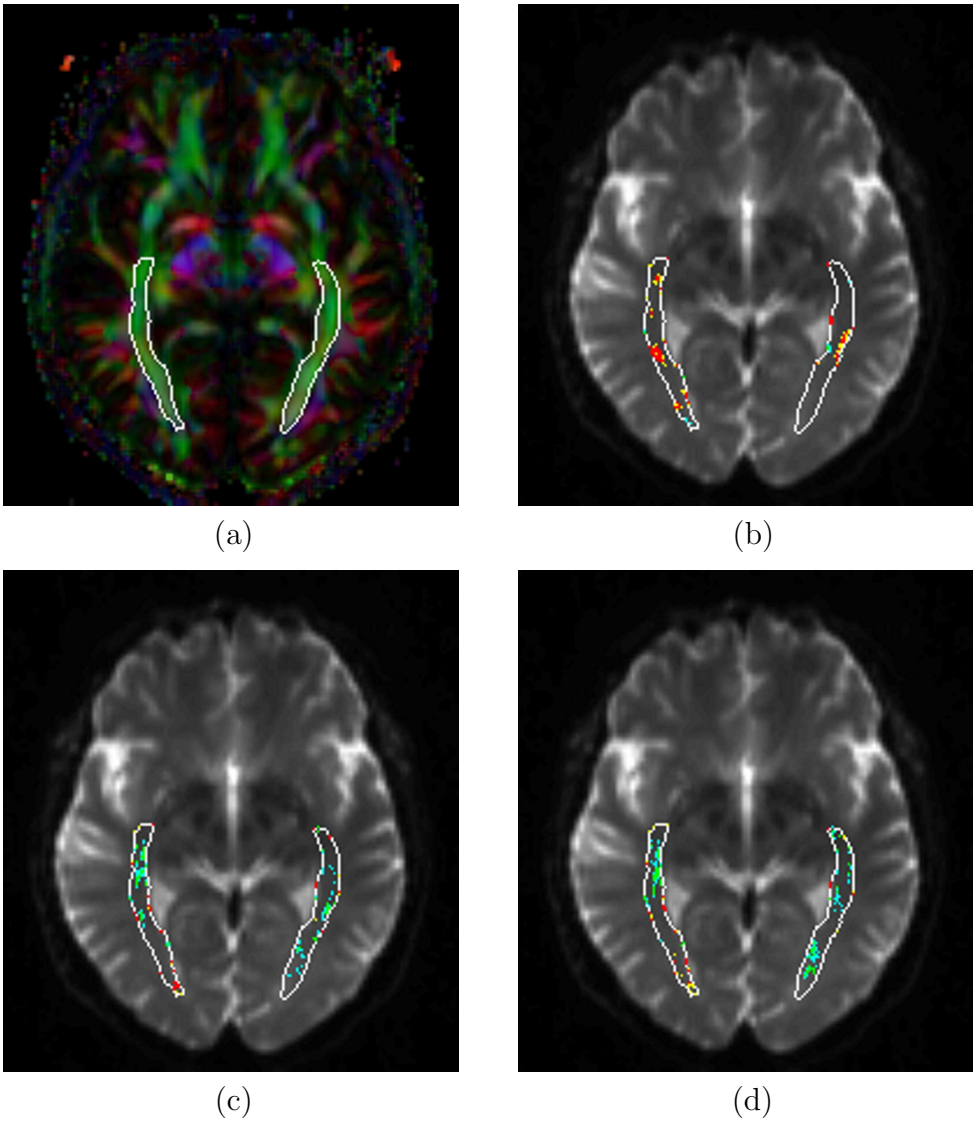

Figure 4: Optic radiation of the reference subject (a) and the significant optic radiation voxels based on the analysis of: (b) Fractional anisotropy (FA), (c) Radial Diffusivity (RD), and (d) Mean Diffusivity (MD) in the presence of glaucoma. The significant regions are marked and the color code is as follows: Red: control group's mean value greater than glaucoma group's mean value with p-value < 0.05, Yellow: control group's mean value greater than glaucoma group's mean value with $0.05 \leq p$-value < 0.1, Green: control group's mean value less than glaucoma group's mean value with p-value < 0.05, Cyan: control group's mean value less than glaucoma group's mean value with $0.05 \leq p$-value < 0.1.

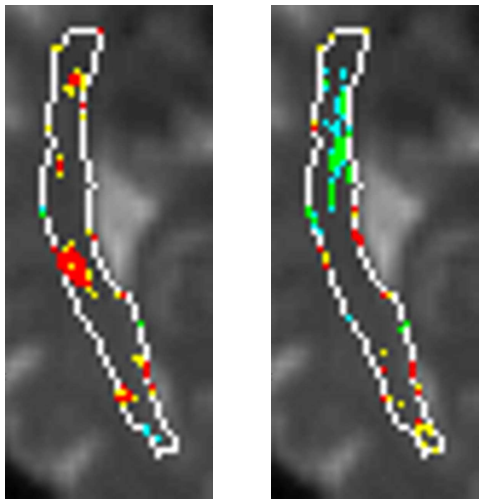

Figure 5: Concentration of significant regions on the right optic radiation according to the fractional anisotropy analysis (left) and according to the mean diffusivity analysis (right). Color code is as follows: Red: control group's mean value greater than glaucoma group's mean value with p-value < 0.05, Yellow: control group's mean value greater than glaucoma group's mean value with $0.05 \leq p$-value < 0.1, Green: control group's mean value less than glaucoma group's mean value with p-value < 0.05, Cyan: control group's mean value less than glaucoma group's mean value with $0.05 \leq p$-value < 0.1.

Table 1: Reliability analysis of the inter-operator configuration of the optic radiation

Group	Overlap(%)		IUratio(%)		Modif. Hausdorff(mm)	
	Mean	SD	Mean	SD	Mean	SD
Glaucoma patients	96.82	2.66	90.22	3.82	0.29	0.13
Normal subjects	88.97	5.38	85.05	5.21	0.61	0.39
All subjects	93.41	5.62	87.98	5.09	0.43	0.31

glaucoma group than in the normal subjects. The proximal part of the right optic radiation near the Meyer loop contained a concentration of significant voxels with increased radial and mean diffusivities. In addition, a significant abnormality region could be observed in the posterior part of the left optic radiation with regard to MD analysis. This region was characterized as well by increased MD. Figure 5 focuses on the optic radiation to show the concentration of voxels with increased MD values in the proximal part. The effect on the AD was scattered and no remarkable localization could be detected (not shown).

5.1. Inter-operator configuration of the optic radiation reliability results

The overlap, IUratio and the MHD of the two experts processed optic radiations were calculated for each subject. The mean and the standard deviation (SD) were calculated for the glaucoma, control groups and all subjects. The results of the reliability analysis are summarized in Table 1. Table 1 shows that the mean overlap in all groups was more than 88%. The correlation between operators as measured by overlap among all subjects is 93.41% with a standard deviation of 5.62%. Subvoxel agreement between operators was indicated by a Hausdorff distance of 0.43 mm for all subjects.

5.2. Registration accuracy evaluation results

The registered optic radiations from all subjects were overlaid on the reference optic radiation. The overlap, IUratio and MHD were calculated for all individual subjects. Table 2 demonstrates the results of the accuracy analysis. The mean residuals (complement of the overlap) from the registration of all subjects did not exceed 7%. For the glaucoma and normal groups, the IUratio means were 87.36% and 89.38%, respectively. Maximum MHD of 0.41 mm for the normal group indicated the subvoxel degree of alignment achieved.

Table 2: Registration accuracy analysis

Group	Overlap(%)		IUratio(%)		Modif. Hausdorff(mm)	
	Mean	SD	Mean	SD	Mean	SD
Glaucoma patients	94.69	2.25	89.38	3.95	0.34	0.13
Normal subjects	93.21	1.55	87.36	1.92	0.41	0.07
All subjects	93.85	1.98	88.24	3.07	0.38	0.11

6. Discussion

The presented framework provides localized abnormality maps of the optic radiation in glaucoma. The application to groups of normal and glaucoma subjects indicates the potential localization capabilities of the system. Furthermore, the system analyzes different relevant diffusion tensor parameters characterizing different properties of the underlying white matter fiber structure of the optic radiation. Thus, regional structural changes of the underlying white matter in the presence of glaucoma could be investigated.

Complexity of the white matter architecture of the human visual system and its variability among subjects complicate the voxel-based analysis. Common VBM approaches aiming to match the highly variable complete brain fiber structure, such as the implementation in statistical parametric mapping (SPM) - (Wellcome. Department of Cognitive Neurology, University College. London, London, UK) and TBSS [38], face the challenge of large registration residuals and misalignments. Therefore, whole brain analysis is avoided. Object oriented analysis (e.g., the work by Xu et al. [47] to analyze the callosal fibers) concentrating on a single object reduces the matching complexity from the whole brain to a specified object. The object oriented approach is adopted in this work with the optic radiation as the object to be analyzed. Using tractography to identify the white matter fibers results in a network of individual fibers which is highly dependent on the user intervention for selecting the seed points or regions of interest. Additionally, the reconstructed fiber tracts may need to be clustered in order to provide fiber bundles. This could lead to another source of errors and affects the voxel-wise comparison. Therefore, a segmentation technique is used for the reconstruction of the optic radiation. So, the optic radiation is represented as a segmented region which facilitates the registration and reduces the sources of errors.

The validity of the results produced by the framework depends on the

accurate identification of the corresponding optic radiation regions in all subjects, the consistency between operators, and the ability to efficiently align the optic radiations to the reference. Therefore, the validation of these issues is crucial to the reliability of the results and to indicate the system efficiency. The optic radiation has a highly complex fiber system [48, 49] that complicates the identification and isolation of its fiber structure. This problem is mitigated by restricting the analysis to the main coherent fiber bundle of the optic radiation. The utilized segmentation algorithm targets the coherent bundle. This is emphasized by the anisotropic filtering and the initialization of the optic radiation using a fractional anisotropy threshold of 0.3. The FA threshold primarily aims to avoid the inclusion of voxels with intravoxel fiber orientational heterogeneity [50] and to disconnect the optic radiation from interfering tracts by the attempt to exclude the voxels representing crossing and branching situations. Moreover, the manual configuration procedure ensures that corresponding optic radiation bundles from different subject are to be compared. i.e., the coherent optic radiation bundles following the LGN and projecting to the primary visual cortex (without the heterogeneous branching tracts) on the LGN-slice.

The optic radiation is automatically determined to eliminate the necessity of user intervention. The manual configuration of the optic radiation is performed by two experts in a simple systematic approach. The LGN is clearly located at the termination region of the optic tract and the beginning of the visual pathway axons projecting to the visual cortex through the identified optic radiation. The branching fibers of the optic radiation near the posterior end of the optic radiation are located in the proximity of the primary visual cortex. The fiber structure in branching and crossing situations is characterized by reduced anisotropy due to the limitation of the diffusion tensor model. Thus, increasing the anisotropy threshold gradually and monitoring the branching region can facilitate the systematic elimination of the highly variable branching bundles. However, the user intervention in this region is limited because the output from the automated segmentation consists mainly of the coherent fiber bundle of the optic radiation. Following these approaches in manually configuring the optic radiation, a high degree of consistency between operators is achieved. Subvoxel inter-operator agreement measured by the modified Hausdorff distance can be attributed to the minimized intervention of operators in the LGN and near the posterior end of the optic radiation. This leaves the majority of the optic radiation unaltered and reduces the average shape deviation.

The robust semi-automated identification of the optic radiation and relying on the remarkable shape similarity for the registration contribute to the high degree of structure alignment. An average overlap between reference and registered optic radiation of greater than 93% is achieved with a subvoxel accuracy of 0.4 mm. Furthermore, glaucoma has been shown to affect tensor-derived parameters such as FA and MD in the optic radiation [7] which in turn affects the whole tensor. Thus, the dependence on the tensor or tensor-derived measures in the registration could result in inconsistency of the analysis among different parameters. This issue is resolved by depending on the segmented optic radiation shape similarity among subjects with and without glaucoma. A registration based on shape similarity ensures consistency when using the obtained transformations to transfer any tensor-derived parameters to the unified space for voxel-wise comparisons.

The decreased FA values of the glaucoma group indicate that the fiber coherency and directionality of water self-diffusion are degraded compared to the normal group. This could be related to an impaired integrity of white matter tracts as suggested by previous studies [9, 10, 12]. The concentration of the significantly decreased FA voxels in the middle between the anterior and posterior parts of the optic radiation demonstrates the localized glaucoma effect in that region. The water diffusion in the direction perpendicular to the PDD is thought to be restricted by the myelin sheaths and the axonal cell membranes [51]. This transverse diffusion is represented by the RD. The process of demyelination in the presence of neurological pathologies was suggested to be associated with reduced RD by Song et al. [11, 16]. The increased radial diffusivity in the glaucoma group concentrated in the proximal part of the right optic radiation suggests a possible demyelination process near the Meyer loop. Mean diffusivity represents the average of the water self-diffusion which is related to the obstacles restricting the diffusion. The locations of significant increase in MD are similar to the results from the RD analysis on the right optic radiation. However, additional major abnormality area can be located in the posterior part of the left optic radiation.

The localization analysis shows approximately symmetric regions on both the middle parts of the left and right optic radiation with respect to FA analysis. However, the abnormalities on the left optic radiation are differently located than the abnormalities on the right optic radiation regarding the RD and MD analyses. The asymmetry in the RD and MD results could be attributed to the hemispheric white matter asymmetry reported previously [52, 53]. Moreover, glaucoma is commonly an advanced age disease [54].

This is reflected in the selection and age matching of the subjects in this study. Aging is associated with brain atrophy which was shown to be asymmetric in both brain hemispheres [55, 34]. As a part of the white matter, the optic radiation could be concerned with the hemispheric asymmetry. Another factor affecting the symmetry of the results could be the limited spatial resolution of the DTI modality which makes the asymmetric acquisition of a complex fiber structure with variable course such as the optic radiation [56] unavoidable.

Recently, the average FA and MD in the optic radiation was reported to be decreased and increased, respectively in the presence of glaucoma [7]. The performed analysis is generally in agreement with these findings and additionally provides a localization map of the deleterious effect of glaucoma on the optic radiation.

The selection of the slice that represents the optic radiation and the manual post-processing may influence the results of the analysis. This influence is reduced by co-registering the DTI images with the anatomical MRI images for the validation of the segmentation and slice selection. However, the slice selection is done by two DTI experts to ensure consistency and reliability of the selection. The small sample size used in this study restricts a strong conclusive statement about the localization results of differences in diffusivity and anisotropy parameters between the normal and glaucoma groups. Potential significant voxels with p-value ≥ 0.05 and < 0.1 are also shown in Figure 4 and Figure 5. The significant regions corresponding to a p-value ≥ 0.05 and < 0.1 are in the neighborhood of the 0.05 p-value analysis regions as shown in Figure 5. Nevertheless, the focus of this work is on the localization framework.

7. Conclusion

In this article a framework is proposed for the localization of the deleterious glaucoma effect on the optic radiation. The system overcomes the complexities of the diffusion tensor imaging and allows for efficient voxel-based morphometric analysis. The framework is based on shape similarity and can be applied to any neurological disease that does not influence the shape topology of the fiber bundle under examination. DTI is a valuable tool for the identification of white matter fibers as well as the characterization and localization of diseases which can assist in understanding the patho-

physiology of neuro-ophthalmologic diseases as glaucoma. The preliminary analysis provides a map of localized fiber abnormalities in the optic radiation associated with glaucoma. Future direction is to conduct a large population study where different glaucoma entities and factors can be examined and differentiated. Following the shape concept introduced in this work, volumetric shape modeling of the optic radiation can be incorporated to perform three dimensional analysis.

Acknowledgements

The authors gratefully acknowledge the funding of German academic exchange service (DAAD) and the Erlangen Graduate School in Advanced Optical Technologies (SAOT) by the German National Science Foundation (DFG) in the framework of the excellence initiative.

References

[1] Fechtner RD, Weinreb RN. Mechanisms of optic nerve damage in primary open angle glaucoma. Surv Ophthalmol 1994; 39(1):23-42.

[2] Quigley HA, Broman AT. The number of people with glaucoma worldwide in 2010 and 2020. The British journal of ophthalmology 2006; 890(3):262-267.

[3] Wichmann W, Müller-Forell W. Anatomy of the visual system. Eur J Radiol 2004; 49(1):8-30.

[4] Remington LA. Clinical anatomy of the visual system, 2nd Edition. Butterworth-Heinemann, 2004. ISBN 0750674903.

[5] Gupta N, Yücel YH. What changes can we expect in the brain of glaucoma patients? Survey of Ophthalmology 2007; 52(6, Supplement 1):S122-S126.

[6] Gupta N, Ang LC, de Tilly LN, Bidaisee L, Yücel YH. Human glaucoma and neural degeneration in intracranial optic nerve, lateral geniculate nucleus, and visual cortex. British Journal of Ophthalmology 2006; 90(6):674-678.

[7] Garaci FG, Bolacchi F, Cerulli A, Melis M, Spanó A, Cedrone C, Floris R, Simonetti G, Nucci C. Optic nerve and optic radiation neurodegeneration in patients with glaucoma: in vivo analysis with 3-T diffusion-tensor MR imaging. Radiology 2009; 252(2):496-501.

[8] Hui ES, Fu QL, So KF, Wu EX. Diffusion tensor MR study of optic nerve degeneration in glaucoma. In: Proceedings of the 29th Annual International Conference of the IEEE Engineering in Medicine and Biology Society (EMBS), 2007. p. 4312-4315.

[9] Pierpaoli C, Jezzard P, Basser PJ, Barnett A, Chiro GD. Diffusion tensor MR imaging of the human brain. Radiology 1996; 201:637-648.

[10] Horsfield MA, Jones DK. Applications of diffusion-weighted and diffusion tensor MRI to white matter diseases - a review. NMR in Biomedicine 2002; 15(7-8):570–577.

[11] Song SK, Sun SW, Ju WK, Lin SJ, Cross AH, Neufeld AH. Diffusion tensor imaging detects and differentiates axon and myelin degeneration in mouse optic nerve after retinal ischemia. NeuroImage 2003; 20(3): 1714–1722.

[12] Hamilton LS, Levitt JG, O'Neill J, Alger JR, Luders E, Phillips OR, Caplan R, Toga AW, McCracken J, Narr KL. Reduced white matter integrity in attention-deficit hyperactivity disorder. Neuroreport (2008); 19(17):1705-1708.

[13] Basser PJ, Mattiello J, Lebihan D. MR diffusion tensor spectroscopy and imaging. Biophysical Journal 1994; 66(1):259-267.

[14] Mori S, Barker PB. Diffusion magnetic resonance imaging: its principle and applications. The Anatomical Record 1999; 257(3):102-109.

[15] Le Bihan D, Mangin JF, Poupon C, Clark CA, Pappata S, Molko N, Chabriat H. Diffusion tensor imaging: concepts and applications. Journal of Magnetic Resonance Imaging 2001; 13(4):534-546.

[16] Song SK, Yoshino J, Le TQ, Lin SJ, Sun SW, Cross AH, Armstrong RC. Demyelination increases radial diffusivity in corpus callosum of mouse brain. NeuroImage 2005; 26(1): 132-140.

[17] Basser PJ, Pierpaoli C. Microstructural and physiological features of tissues elucidated by quantitative-diffusion-tensor MRI. Journal of magnetic resonance, Series B 1996; 111(3):209-219.

[18] Basser PJ, Jones DK. Diffusion-tensor MRI: theory, experimental design and data analysis - a technical review. NMR Biomed 2002; 15(7-8):456-467.

[19] Nucifora PG, Verma R, Lee SK, Melhem ER. Diffusion-tensor MR imaging and tractography: exploring brain microstructure and connectivity. Radiology 2007; 245(2):367-384.

[20] Mori S, Oishi K, Jiang H, Jiang L, Li X, Akhter K, Hua K, Faria AV, Mahmood A, Woods R, Toga AW, Pike GB, Neto PR, Evans A, Zhang J, Huang H, Miller MI, van Zijl P, Mazziotta J. Stereotaxic white matter atlas based on diffusion tensor imaging in an ICBM template. Neuroimage 2008; 40(2):570-582.

[21] Dong Q, Welsh RC, Chenevert TL, Carlos RC, Maly-Sundgren P, Gomez-Hassan DM, Mukherji SK. Clinical applications of diffusion tensor imaging. Journal of Magnetic Resonance Imaging 2004; 19(1):6-18.

[22] Moseley ME, Cohen Y, Mintorovitch J, Chileuitt L, Shimizu H, Kucharczyk J, Wendland MF, Weinstein PR. Early detection of regional cerebral ischemia in cats: comparison of diffusion- and T2-weighted MRI and spectroscopy. Magnetic Resonance in Medicine 1990; 14(2):330-346.

[23] Lansberg MG, Norbash AM, Marks MP, Tong DC, Moseley ME, Albers GW. Advantages of adding diffusion-weighted magnetic resonance imaging to conventional magnetic resonance imaging for evaluating acute stroke. Arch Neurol 2000; 57(9):1311-1316.

[24] Huang J, Friedland RP, Auchus AP. Diffusion tensor imaging of normal-appearing white matter in mild cognitive impairment and early alzheimer disease: preliminary evidence of axonal degeneration in the temporal lobe. American Journal of Neuroradiology 2007; 28(10):1943-1948.

[25] Chen T, Lin C, Chen Y, Liu H, Hua M, Huang Y, Chiu M. Diffusion tensor changes in patients with amnesic mild cognitive impairment and

various dementias. Psychiatry Research: Neuroimaging 2009; 173(1):15-21.

[26] Henry RG, Oh J, Nelson SJ, Pelletier D. Directional diffusion in relapsing-remitting multiple sclerosis: a possible in vivo signature of Wallerian degeneration. Journal of Magnetic Resonance Imaging 2003; 18(4):420-426.

[27] Staempfli P, Rienmueller A, Reischauer C, Valavanis A, Boesiger P, Kollias S. Reconstruction of the human visual system based on DTI fiber tracking. Journal of Magnetic Resonance Imaging 2007; 26(4):886-893.

[28] Sherbondy AJ, Dougherty RF, Napel S, Wandell BA. Identifying the human optic radiation using diffusion imaging and fiber tractography. J Vis 2008; 8(10):12.1-11.

[29] El-Rafei A, Engelhorn T, Waerntges S, Doerfler A, Hornegger J, Michelson G. Automatic segmentation of the optic radiation using DTI in healthy subjects and patients with glaucoma. In: J.M.R.S. Tavares, R.M.N. Jorge (eds.) Computational Vision and Medical Image Processing, Computational Methods in Applied Sciences 2011; 19:1-15. Springer Netherlands.

[30] Valsasina P, Rocca MA, Agosta F, Benedetti B, Horsfield MA, Gallo A, Rovaris M, Comi G, Filippi M. Mean diffusivity and fractional anisotropy histogram analysis of the cervical cord in MS patients. NeuroImage 2005; 26(3):822-828.

[31] Nave RD, Foresti S, Pratesi A, Ginestroni A, Inzitari M, Salvadori E, Giannelli M, Diciotti S, Inzitari D, Mascalchi M. Whole-brain histogram and voxel-based analyses of diffusion tensor imaging in patients with leukoaraiosis: correlation with motor and cognitive impairment. AJNR Am J Neuroradiol 2007; 28(7):1313-1319.

[32] Ciccarelli O, Toosy AT, Hickman SJ, Parker GJM, Wheeler-Kingshott CAM, Miller DH, Thompson AJ. Optic radiation changes after optic neuritis detected by tractography-based group mapping. Human Brain Mapping 2005; 25(3):308-316.

[33] Thivard L, Pradat P, Lehéricy S, Lacomblez L, Dormont D, Chiras J, Benali H, Meininger V. Diffusion tensor imaging and voxel based morphometry study in amyotrophic lateral sclerosis: relationships with motor disability. Journal of Neurology, Neurosurgery & Psychiatry 2007; 78(8):889-892.

[34] Ardekani S, Kumar A, Bartzokis G, Sinha U. Exploratory voxel-based analysis of diffusion indices and hemispheric asymmetry in normal aging. Magnetic Resonance Imaging 2007; 25(2):154-167.

[35] Takao H, Abe O, Yamasue H, Aoki S, Kasai K, Sasaki H, Ohtomo K. Aging effects on cerebral asymmetry: a voxel-based morphometry and diffusion tensor imaging study. Magnetic Resonance Imaging 2010; 28(1):65-69.

[36] Takao H, Abe O, Yamasue H, Aoki S, Kasai K, Ohtomo K. Cerebral asymmetry in patients with schizophrenia: a voxel-based morphometry (VBM) and diffusion tensor imaging (DTI) study. Journal of Magnetic Resonance Imaging 2010; 31(1):221-226.

[37] Jones DK, Symms MR, Cercignani M, Howard RJ. The effect of filter size on VBM analyses of DT-MRI data. NeuroImage 2005; 26(2):546-554.

[38] Smith SM, Jenkinson M, Johansen-Berg H, Rueckert D, Nichols TE, Mackay CE, Watkins KE, Ciccarelli O, Cader MZ, Matthews PM, Behrens TEJ. Tract-based spatial statistics: voxelwise analysis of multi-subject diffusion data. NeuroImage 2006; 31(4):1487-1505.

[39] Arsigny V, Fillard P, Pennec X, Ayache N. Log-Euclidean metrics for fast and simple calculus on diffusion tensors. Magnetic Resonance in Medicine 2006; 56(2):411-421.

[40] Perona P, Malik J. Scale-space and edge detection using anisotropic diffusion. IEEE Transactions on Pattern Analysis and Machine Intelligence 1990; 12(7): 629–639.

[41] Lenglet C, Rousson M, Deriche R. DTI segmentation by statistical surface evolution. IEEE Transactions on Medical Imaging 2006; 25(6):685-700.

[42] Wakana S, Jiang H, Nagae-Poetscher LM, van Zijl PC, Mori S. Fiber tract-based atlas of human white matter anatomy. Radiology 2004; 230(1):77-87.

[43] Westin CF, Maier SE, Mamata H, Nabavi A, Jolesz FA, Kikinis R. Processing and visualization for diffusion tensor MRI. Medical Image Analysis 2002; 6(2):93-108.

[44] Rueckert D, Sonoda LI, Hayes C, Hill DLG, Leach MO, Hawkes DJ. Nonrigid registration using free-form deformations: application to breast MR images. IEEE Transactions on Medical Imaging 1999; 18(8):712-721.

[45] John JP, Wang L, Moffitt AJ, Singh HK, Gado MH, Csernansky JG. Inter-rater reliability of manual segmentation of the superior, inferior and middle frontal gyri. Psychiatry Research: Neuroimaging 2006; 148(2-3):151-163.

[46] Dubuisson MP, Jain AK. A modified Hausdorff distance for object matching. In: Proceedings of the 12th IAPR International Conference on Pattern Recognition, Conference A: Computer Vision & Image Processing, Vol. 1. 1994. p. 566-568.

[47] Xu D, Mori S, Solaiyappan M, van Zijl PCM, Davatzikos C. A framework for callosal fiber distribution analysis. NeuroImage 2002; 17(3):1131-1143.

[48] Türe U, Yasargil MG, Friedman AH, Al-Mefty O. Fiber dissection technique: lateral aspect of the brain. Neurosurgery 2000; 47(2):417-427.

[49] Sincoff EH, Tan Y, Abdulrauf SI. White matter fiber dissection of the optic radiations of the temporal lobe and implications for surgical approaches to the temporal horn. J Neurosurg 2004; 101(5):739-746.

[50] Tuch DS, Reese TG,Wiegell MR, Makris N, Belliveau JW,Wedeen VJ. High angular resolution diffusion imaging reveals intravoxel white matter fiber heterogeneity. Magnetic Resonance in Medicine 2002; 48(4):577-582.

[51] Beaulieu C. The basis of anisotropic water diffusion in the nervous system - a technical review. NMR in Biomedicine 2002; 15(7-8):435–455.

[52] Peled S, Gudbjartsson H, Westin CF, Kikinis R, Jolesz, FA. Magnetic resonance imaging shows orientation and asymmetry of white matter fiber tracts. Brain Research 1998; 780(1):27–33.

[53] Park HJ, Westin CF, Kubicki M, Maier SE, Niznikiewicz M, Baer A, Frumin M, Kikinis R, Jolesz FA, McCarley RW, Shenton ME. White matter hemisphere asymmetries in healthy subjects and in schizophrenia: a diffusion tensor MRI study. NeuroImage 2004; 23(1):213–223.

[54] Tuck MW and Crick RP. The age distribution of primary open angle glaucoma. Ophthalmic Epidemiology 1998; 5(4):173–183.

[55] Dolcos F, Rice HJ, Cabeza R. Hemispheric asymmetry and aging: right hemisphere decline or asymmetry reduction. Neuroscience & Biobehavioral Reviews 2002; 26(7):819–825.

[56] Hofer S, Karaus A, Frahm J. Reconstruction and dissection of the entire human visual pathway using diffusion tensor MRI. Frontiers in Neuroanatomy 2010; 13:4–15.